


Assisted percolation of slow-spreading mutants in heterogeneous environmentsThomas Tunstall^{1,2}, Tim Rogers³, and Wolfram Möbius^{1,2,*}¹*Living Systems Institute, Faculty of Health and Life Sciences, University of Exeter, Exeter, EX4 4QD, United Kingdom*²*Physics and Astronomy, Faculty of Environment, Science and Economy, University of Exeter, Exeter, EX4 4QL, United Kingdom*³*Center for Networks and Collective Behaviour, Department of Mathematical Sciences, University of Bath, Bath, BA2 7AY, United Kingdom* (Received 6 March 2023; revised 1 August 2023; accepted 11 August 2023; published 4 October 2023)

Environmental heterogeneity can drive genetic heterogeneity in expanding populations; mutant strains may emerge that trade overall growth rate for an improved ability to survive in patches that are hostile to the wild type. This evolutionary dynamic is of practical importance when seeking to prevent the emergence of damaging traits. We show that a subcritical slow-spreading mutant can attain dominance even when the density of patches is below their percolation threshold and predict this transition using geometrical arguments. This work demonstrates a phenomenon of “assisted percolation”, where one subcritical process assists another to achieve supercriticality.

DOI: [10.1103/PhysRevE.108.044401](https://doi.org/10.1103/PhysRevE.108.044401)**I. INTRODUCTION**

Pesticides are used to control crop pests, antimicrobials to eliminate microbes, and cancer drugs to contain tumors. The emergence of mutants that are resistant to these agents is a major concern in all these scenarios [1–3]. The double-edged sword of use and control on the one hand, and loss of efficacy through the emergence of resistance is widely acknowledged, but we know relatively little about the role spatial structure plays in the dynamics of resistance emergence. Research on the effects of spatial structure on resistance emergence include the effects of compartmentalisation, for example in the human body [4,5], and the effect of gradients on evolutionary dynamics [6,7]. Research on the durability of genetically controlled plant resistance to pests in fields of crops is conceptually very similar [8]. These studies focus on the emergence of mutants which overcome the efficacy of control agents or genetic protection; how these mutants then spread in a complex environment is not understood.

II. MODEL AND PHENOMENOLOGY

We here address this question from a theoretical physics perspective, for a two-dimensional environment with isolated patches that can be thought of as being protected by the control agent. We generalize the Type C variant [9] of the Eden model [10], a lattice-based model for growth which is suitable for spread in heterogeneous environments, intrinsically incorporates stochasticity, and whose computational efficiency matches the requirement to investigate large systems and many replicates [Figs. 1(a) and 1(b), and S1, and

expanding on previous work [11–15], see the Supplemental Material [16]).

Incorporating environmental heterogeneity, mutation, and selection in a two-species Eden model, we consider a hexagonal lattice of sites. Unoccupied sites can be either “background” or “patch” varieties, whilst occupied sites are either “wild-type” (WT) or “mutant” (M) [Fig. 1(a)]. During each time step, an occupied site on the population frontier is selected to reproduce, at which point offspring of the same type as the parent are placed in a random unoccupied neighboring site; only M are able to reproduce into a patch site, to represent their resistance to the control measure. During reproduction, there is a finite probability μ of mutation from WT to M [Fig. 1(a)], but no mutations from M to WT can occur. Selection of WT or M sites to reproduce occurs with probability proportional to their “fitness” which is taken to be 1 for WT and $0 < F < 1$ for M, modeling the cost of resistance [Fig. 1(b)].

In finite-width spreading fronts, M will eventually come to dominate as this is the only absorbing state. However, the timescale can vary dramatically: Even in the absence of patch sites, one can distinguish a supercritical phase of fast fixation and a subcritical phase of exponentially slow fixation [12]. Below criticality, small clusters of M appear, but typically die out before coalescing with others. Increasing M fitness or mutation rate causes these clusters to grow in size or frequency, respectively, to the point where multiple coalescence events can occur and the M population becomes supercritical [Fig. S1(c)]. For a similar model with a flat expanding front [Fig. S2(a)], the dynamics fall into the directed percolation universality class [17]. The roughness inherent to the Eden model we use as the basis for our generalized model greatly perturbs us from the directed percolation universality class. Kuhr *et al.* [12] performed phenomenological analysis on the Eden model to determine the phase boundary at $\mu \approx p^*(1 - F)^{1.4}$ with $p^* \approx 0.407$ [12]. Generally, for a given mutation rate, we can define the critical fitness $F_c(\mu)$. As a general result, M dominates quickly if $F > F_c(\mu)$.

*w.moebius@exeter.ac.uk

Published by the American Physical Society under the terms of the [Creative Commons Attribution 4.0 International](https://creativecommons.org/licenses/by/4.0/) license. Further distribution of this work must maintain attribution to the author(s) and the published article’s title, journal citation, and DOI.

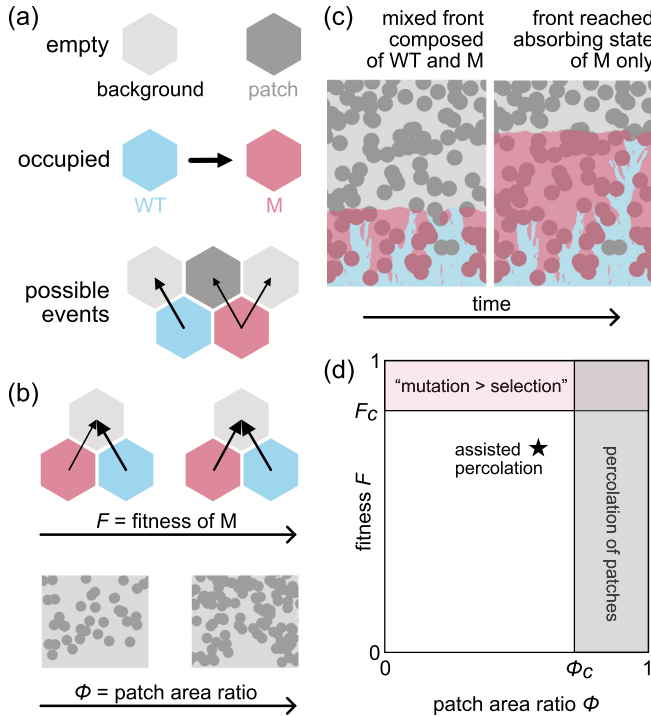


FIG. 1. (a) Rules underlying the generalized Eden model. The possible reproduction events of the next simulation step are represented by arrows. See also Figs. S1(a) and (b). (b) Visualization of the effects of increasing fitness F of M and patch area ratio ϕ . (c) M dominates in an expanding front in the presence of treated patches (dark circles) in which only M [red (dark gray)] survive. The population propagates from bottom to top (see color version to access all information). See the video in S1 [16] for a depiction of the full simulation. (d) Sketch of phase diagram, for sufficiently high fitness $F > F_c$ and patch area $\phi > \phi_c$, dominance of M is expected. Parameters for simulation in panel (c) lie outside of these regions, indicating a richer structure to the phase diagram in which assisted percolation takes place.

We incorporate macroscopic environmental heterogeneity into this model by arranging treated patch sites into circular patches of fixed radii, either randomly placed [Fig. 1(b)] or in a lattice arrangement. This type of heterogeneity differs from that of previous work [15] by acting asymmetrically on different genotypes: They act as hard boundaries for WT [18], but are transparent to M. For random placements, continuum percolation theory gives a critical threshold of $\phi_c^\circ \approx 0.68$ [19] for the ratio ϕ of area covered by patches to total area; for $\phi > \phi_c^\circ$ the patches themselves form a percolating cluster allowing only M lineages to survive. Therefore, for a given mutation rate, M dominates either if $F > F_c$ or $\phi > \phi_c^\circ$. The example shown in Fig. 1(c) demonstrates, however, that these are merely sufficient conditions. Rapid domination of M can occur with both fitness and patch area ratio being significantly lower than the critical thresholds. We aim to examine the full structure of the phase diagram sketched in Fig. 1(d).

III. ESCAPE REGIONS

Close examination of simulations such as that presented in Fig. 1(c) and the video in S1 [16] reveals the mechanisms

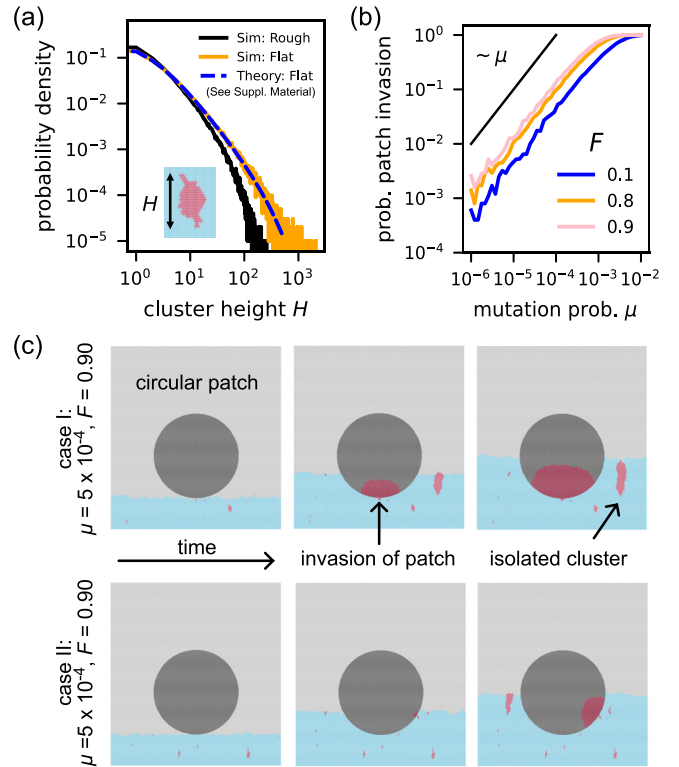


FIG. 2. (a) Cluster height distributions for the Eden model (rough front) and a flat-front model, both obtained from simulations, together with the analytical result for flat fronts for $F = 0.90$. Inset: Typical cluster in our model. (b) Probability of an isolated patch being invaded as a function of mutation rate μ for different fitness values F . Black line represents a linear relationship. (c) Two examples for how clusters invade a patch with $\mu = 5 \times 10^{-4}$, $F = 0.90$: (case I) Invasion from the bottom and (case II) invasion from the bottom right. In both cases, M inside the patch lags the WT front outside. See the videos in S2 and S3 [16] for a depiction of the full simulations.

driving M domination. When small M clusters intersect with a treated patch they spread through it and emerge from the other side ahead of the faster spreading WT population that is forced to take a longer route around the patch acting as an obstacle. If the “escape region” beyond a treated patch is large enough, it will intersect with another patch and M population growth will continue. This is an effect of “assisted percolation” as we will explore later. To determine the boundary of the fast fixation phase, it is therefore necessary to (i) compute the expected size of escape regions and (ii) understand the effective between-patch percolation process.

At first glance, the statistics of lone M clusters are important to this problem. These statistics are remarkably complex; to our knowledge, only the scaling behaviours have been determined for a square lattice in the literature [12]. However, as demonstrated in Fig. 2(a), the vast majority of isolated M clusters in the regime considered here are much smaller than the typical size of the patches (area $\sim 10^3$). We have undertaken further analytical work in determining the dimensions of the lone M clusters for an equivalent model with a flat front (expanding and building on previous work [20–23], see

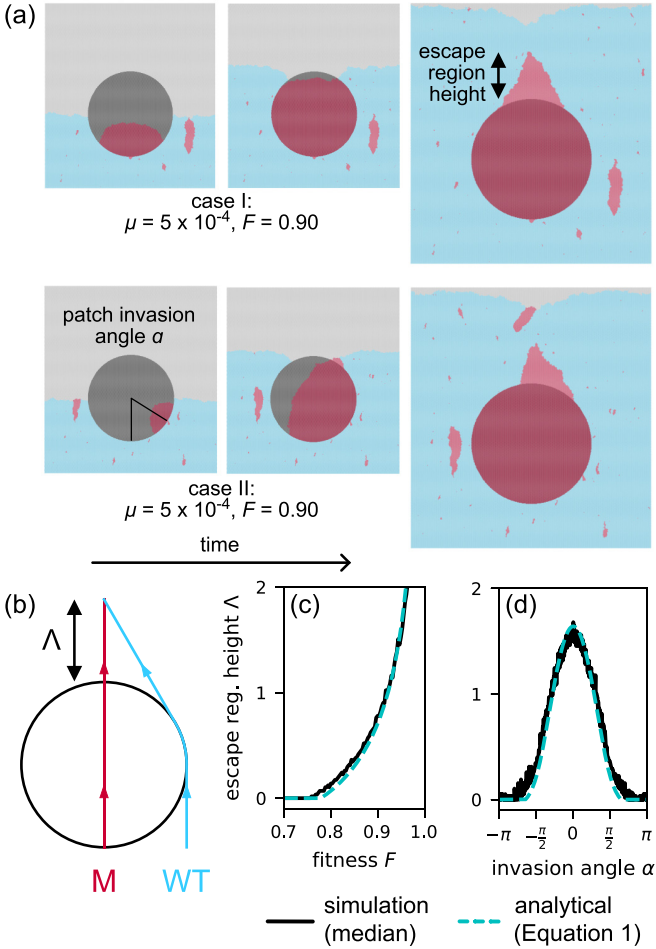


FIG. 3. (a) Continuing the time evolution of the patch invasions in Fig. 2(c) with emphasis on the escape region. See the videos in S2 and S3 [16] for depiction of the full simulations. (b) Sketch of the deterministic escape region height, found by equating the time taken for M to pass through the patch with the time taken for WT to pass around the patch to the same point. (c) Normalized escape region height as a function of fitness F for patch invasion angle $\alpha = 0$. Black data points: Median of simulation results, cyan (light gray) dashed line: Geometrical prediction. (d) Like panel (c) but as a function of patch invasion angle α for fitness $F = 0.95$.

the Supplemental Material [16]). How often these clusters lead to invasion of a patch depends on mutation rate and fitness. Figure 2(b) illustrates that the probability to invade a patch increases linearly and then saturates with increasing mutation rate as expected; similarly, a higher fitness results in higher probability of invasion. To abstract from both the sizes of isolated clusters and their abundance, we focus on the consequences of individual patches being invaded. In this way, we capture the long-term behavior of the “thermodynamic limit” of a large system of patches with rare mutations.

While clusters are small relative to the patch’s radius when outside a patch, they can spread unimpaired through the patch, leading to large domains within patches, as seen in Fig. 2(c). These domains may eventually become trapped within or escape the patch. Examples of the latter are shown in Fig. 3(a),

where the invading M domain spreads upward through the patch and is able to escape before it can be headed off by WT. We expect the existence of the escape region and, if applicable, its height to depend on the patch invasion angle α (which acts as the starting point for a race between M and WT strains), M’s fitness F (the relative speed of M), as well as stochastic effects. In fact, simulations with invasions seeded at different locations of the patch’s boundary show that the median of escape region height increases with fitness F and decreases with absolute value of the invasion angle, i.e., it is largest if the invasion occurs at the bottom of the patch [black line, Figs. 3(c) and 3(d)].

To understand this dependence quantitatively we turn to geometric arguments. Previous work has characterized front shape of a population encountering an obstacle in the absence of mutations and if front speed is the same everywhere outside the obstacle [13]. There, the front shape was determined as the set of all points that can be reached within a given time. Here we aim to find the point along the symmetry axis which is reached at the same time by WT expanding around the patch (with relative speed 1) and M expanding through the patch (with relative speed F), Figs. 3(b) and S3. Measured in units of patch radius, we find that the typical maximum extent of escape regions $\Lambda(F, \alpha)$ solves the following equation (for $|\alpha| < \frac{\pi}{2}$, see the Supplemental Material [16] for derivation):

$$\frac{1}{F} \sqrt{1 + 2(1 + \Lambda) \cos |\alpha| + (1 + \Lambda)^2} = \cos |\alpha| + \arcsin \frac{1}{1 + \Lambda} + \sqrt{(1 + \Lambda)^2 - 1}. \quad (1)$$

If a real, positive solution does not exist, this means that M was cut off immediately and did not escape, thus $\Lambda = 0$. The numerical solution of Eq. (1) describes the simulation data well when varying fitness F or patch invasion angle α [Figs. 3(c) and 3(d)].

IV. INTERACTION BETWEEN PATCHES

Having developed an understanding of the escape region from a single patch, we can examine the macrostructure emergent in a system of many randomly distributed patches. Three expansions for mutation rate $\mu = 10^{-3}$ and with varying fitness F and patch area ratio ϕ are displayed in Fig. 4(a). For low F and ϕ , patches and/or escape regions rarely overlap; when either of these values crosses a threshold, overlaps appear to lead to a growth of the fraction of M and ultimately domination of the front. To predict the patch area ratio at which this transition takes place, we estimate the percolation threshold for patches including escape regions [Fig. 4(b)].

Given the nature of the system with a front mainly propagating from bottom to top, with M clusters typically being oriented in the direction of overall front propagation, we expect most invasions to occur at the bottom of the patch [invasion angle $\alpha \approx 0$, Figs. 3(a) and 3(b)]. In this case, macrostructures consist of the patch and a symmetric escape region with height $\Lambda(F, \alpha = 0)$. Continuing to measure length in units of radius R , the macrostructures have width 2 and height $2 + \Lambda$. These are approximated by aligned ellipses of semiminor axis 1 and semimajor axis $(2 + \Lambda)/2$.

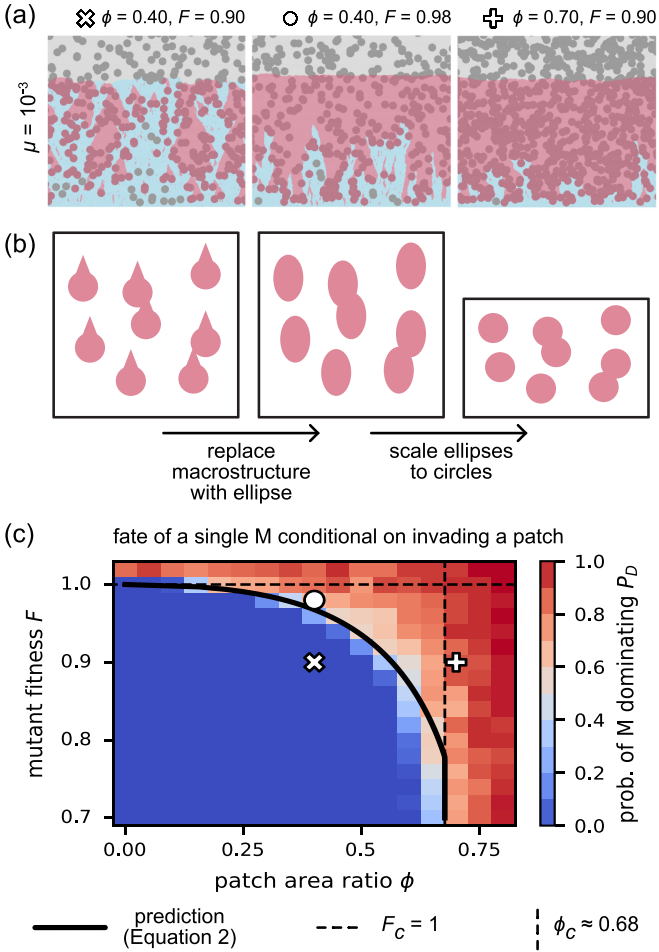


FIG. 4. (a) Three snapshots of simulations for different values of fitness F and patch area ratio ϕ and $\mu = 10^{-3}$. See the videos in S4–S6 [16] for depictions of the full simulations. (b) Description of the approach and approximation used to determine whether, for given fitness F and patch area ratio ϕ , the system displays subcriticality (M extinction) or supercriticality (M domination) in the case of a single mutation event. (Left) The patches are randomly distributed. With each patch invaded from below, fitness-dependent escape regions form. (Center) The macrostructure consisting of patch and escape region is approximated by an ellipse. (Right) Rescaling the height of the system allows one to recover the case of overlapping discs for which the percolation threshold is known. The system is subcritical below and supercritical above the percolation threshold. (c) Grid heat map of the probability of M dominating the front determined by simulations in which the mutation rate is set to zero after the first mutation occurs. The black line indicates the prediction of the boundary by Eq. (2), where the region of low probability is below the curve and the region of higher probability is above the curve. Horizontal and vertical dashed lines indicate the transition by the mutation-selection process and percolation threshold of patches, respectively.

The percolation transition for vertically aligned ellipses can be obtained from the percolation transition for circles by rescaling the height of the system such that ellipses become circles.

As detailed in the Supplemental Material [16], we can thus express the critical area ratio of patches ϕ_c^* assisting percolation of the slow-spreading mutants by the critical area ratio of

discs in two dimensions, $\phi_c^\circ \approx 0.68$ [19,24]:

$$\phi_c^*(F) = 1 - (1 - \phi_c^\circ)^{2/(2+\Lambda(F))}, \quad (2)$$

where we explicitly denote that ϕ_c^* depends on fitness F because the (rescaled) escape region height Λ depends on F . Note that Eq. (2) reduces to $\phi_c^*(F) = \phi_c^\circ$ for $\Lambda(F) = 0$ as expected. When F is sufficiently small such that no escape region is expected to arise, the transition line becomes vertical as seen in Fig. 4(c). In this argument we demonstrate that supercriticality can be achieved via the dynamics of a subcritical M population being perturbed by the presence of a subcritical area ratio of patches, hence the term “assisted percolation”.

To test how well Eqs. (1) and (2) capture the transition from subcritical to supercritical regime, we simulated the system 50 times for a wide range of fitness values F and patch area ratios ϕ with patch radius $R = 40$ and computed the probability P_D with which M fixes at the front conditional on invasion of one patch (Fig. 4, see the Supplemental Material [16] for details). To ensure that we only study the fate of a single mutation, the mutation rate is set to zero after the first mutation occurs. To ensure that we have studied the case where M has invaded a patch, we keep track of the number of M on the population frontier: If this value ever exceeds the diameter of a patch, we can be confident that a patch has been invaded. If a cluster collapses before this threshold is met, the simulation is rerun for the same distribution of patches. The transition region is characterized by P_D being distinct from zero and one and is thus indicated by lighter colors. $\phi_c^*(F)$ in Eq. (2), indicated as a black line, indeed captures this transition region very well. This means that the description of macrostructures interacting with each other and the approximations made capture the dynamics of the system very well.

V. PATCHES ARRANGED IN A HEXAGONAL LATTICE

Motivated by wanting to further explore the applicability of these geometric arguments, and to develop a symmetrical patch distribution which can be designed to inhibit M domination, we considered patches organized on a hexagonal lattice. We chose the hexagonal lattice because it allows for the densest packing of patches [25] and because of its high symmetry. Once again we display three expansions for mutation rate $\mu = 10^{-3}$ with varying fitness F and patch area ratio ϕ (Fig. 5(a)), and observe that a threshold exists for both of these variables which separates subcriticality from supercriticality.

In the hexagonal lattice, the separation between the surfaces of adjacent patches, S , is related to the patch area ratio by $\phi = 2\pi R^2/(\sqrt{3}(2R + S)^2)$. As in the case of randomly oriented patches, we were interested in the critical patch area ratio, ϕ_c° , above which M quickly dominates.

For $S = 0$, neighboring patches are in contact and there is no path for WT to propagate vertically. Conversely, for sufficiently large S , WT can propagate vertically unhindered by obstacles, and isolated M clusters will become enclosed by WT for any $F < 1$. The presence of these vertical paths depends upon the orientation of the lattice relative to the population front. For the case where nearest-neighbor patches are horizontally adjacent (the “horizontal alignment”, as seen in Fig. S4(a), upper), vertical channels occur for large

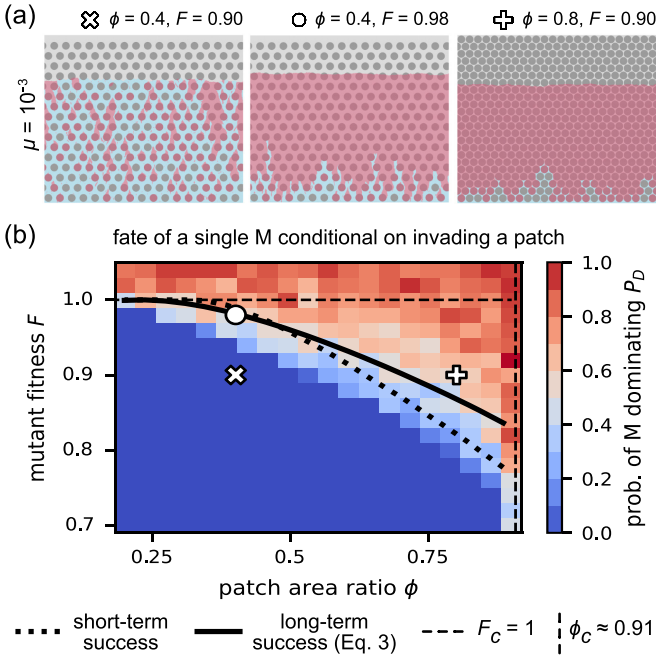


FIG. 5. (a) Three snapshots of simulations for different combinations of ϕ and F for $\mu = 10^{-3}$. See the videos in S7–S9 [16] for depictions of the full simulations. (b) Grid heat map of the probability of M dominating the front, determined by simulation in which the mutation rate is set to zero after the first mutation occurs. Dotted black line indicates a numerical prediction generated by consideration for short-term success, solid black line indicates analytical prediction generated by consideration for long-term success. The region of low probability is at the bottom left, and the region of higher probability is above the curves. Horizontal and vertical dashed lines indicate the transition by the mutation-selection process and overlap of patches, respectively.

separations of $S \geq 2R$. For the case where nearest neighbor patches are vertically adjacent (the “vertical alignment”, as seen in Fig. S4(a), lower) vertical channels are present for $S \geq (\frac{4}{\sqrt{3}} - 2)R \approx 0.31R$. We focus on the horizontal alignment as it provides a bigger path length advantage to M. In this case, the critical patch area ratio ϕ_c^\square is bounded as $\phi(S = 2R) = \frac{\pi}{8\sqrt{3}} \approx 0.23 \leq \phi_c^\square \leq \phi(S = 0) = \frac{\pi}{2\sqrt{3}} \approx 0.91$ given the arguments above.

To estimate the regime of assisted percolation, i.e., ϕ_c^\square , more precisely, we considered two different rationales, both sketched in Fig. S4 and detailed in the Supplemental Material [16]: First, we asked whether, in the short term, an escape region can lead to invasion of an adjacent downstream patch. This could lead to propagation of M through rows of patches given an initially expanding M cluster. However, it is difficult to prove whether this would prompt a continually expanding M cluster, as there is an asymmetry between the invasion of downstream patches and the initial patch: Whereas we assume the initial patch is invaded from the bottom of the patch, there is no guarantee that the downstream patches will also be invaded from the bottom. The second approach is to determine whether, in the long term, M can propagate faster vertically through the lattice of patches than WT. This approach is symmetrical across all rows and does not depend on

the initial invasion of a patch. Focusing here on the long-term consideration, ϕ_c^\square can be determined by comparing the path length of WT snaking around patches while M passing straight through, similar to the computation of escape region height above. This yields the analytical result for the corresponding critical fitness F_c^\square :

$$F_c^\square(\phi) = \frac{\sqrt{3}}{2} \frac{2 + \eta(\phi)}{\sqrt{\eta(\phi)^2 + 4\eta(\phi) + 2(\frac{\pi}{3} - \arccos \frac{2}{2+\eta(\phi)})}} \quad (3)$$

with η the ratio of separation S to patch radius R , which is a function of patch area ratio, $\eta(\phi) = \sqrt{\frac{2\pi}{\sqrt{3}\phi}} - 2$.

To test these predictions, we performed simulations investigating the fate of a single mutation and, as before, determined the probability of M dominating from 50 replicates. Figure 5(b) confirms the existence of the assisted percolation regime in which M dominates but for which M propagates slower than WT ($F < 1$) and in which no vertical paths not overlapping with patches exist. Note that compared to the case of randomly distributed patches [Fig. 4(c)], for a given patch area ratio the fitness of M needs to be higher to ensure M domination. The transition computed numerically for the short-term argument (see Supplemental Material [16]) and the transition based on the analytical long-term argument [Eq. (3)] both adequately capture the transition to assisted percolation. This highlights that geometric arguments alone can predict the behavior of the intrinsically stochastic system. Further research, however, is necessary to disentangle whether short- or long-term prediction or another approach are best suited to predict the dynamics of the system.

VI. CONCLUSION AND DISCUSSION

We addressed the question of how mutants spread in a complex environment of control agents using a generalized Eden model with mutations in a heterogeneous environment. In the analysis, we incorporated results from disparate analyses of the Eden model (mutation-selection process in the absence of patches [12] and the perturbation of a front in the presence of obstacles [13,18]). We demonstrated the phenomenon of assisted percolation where two subcritical processes, mutation selection and overlap of patches, assist each other to achieve supercriticality. The regime within which assisted percolation occurs depends on the distribution of patches, i.e., the parameters of environmental heterogeneity of the system.

There are three parameters of the system we did not systematically vary, but whose effects we can nevertheless predict. First, we chose mutation rate to be very low; specifically, we systematically investigated the fate of a single M site for patches organized randomly [Fig. 4(c)] and in a hexagonal lattice [Fig. 5(b)]. With increasing mutation rate we expect M to dominate for a larger range of parameter pairs of fitness and patch area ratio, (F, ϕ) . Conversely, introducing back mutations would leave the system without an absorbing state. Determining the resulting steady state ratio of WT and M at the front is a question for further research. We did not systematically vary the radius of patches, measured in units of the lattice constant. Our predictions are based on geometric arguments relying on front propagation of WT and M [e.g.,

Fig. 3(b), Eq. (1)]. Stochastic effects should become less important on larger scales; we therefore predict the phenomenon of assisted percolation and specifically the prediction of the transition between WT and M dominating to be valid for patches of larger radius. For significantly smaller radii, we expect the geometrical description to break down.

Our findings suggest two broader avenues for further research. First, in the control of pests, microbes, and tumors, the emergence of resistance to the control agent can lead to failure of control. Comparing Fig. 4(c) to Fig. 5(b) demonstrates that the choice of patch distribution strongly affects how quickly M dominates the front, which we here use as a proxy for failure for control. Tackling the complex optimization problem of preventing M domination for given patch area ratio but arbitrary organization of patches would be a natural next step in the translation of this work to an applied setting.

Second, we have demonstrated the existence of the dynamic of assisted percolation in a generalized version of a popular surface growth model. We speculate that the phenomenon might be relevant to a range of other systems. This may not be limited to systems with short-range invasion as considered here. Long-range dispersal may provide a further

benefit for M, but limited dispersal compared to WT may hinder its spread. Extending our generalized model to include long-range dispersal of both WT and M [26,27] would be the next step.

In particular we expect that further examples may be found in the field of complex networks where, for example, a weak signal might achieve long-range transmission through a subcritical set of amplifying nodes; potentially important applications to epidemiology and social dynamics are not hard to imagine.

The code with instructions on how to reproduce individual figures is available in Ref. [28].

ACKNOWLEDGMENTS

We are grateful to Dibyendu Dutta for discussions and feedback on the manuscript. T.T. acknowledges support by the EPSRC DTP and Syngenta Crop Protection. W.M. acknowledges support by the BBSRC via BBSRC-NSF/BIO Grant BB/V011464/1. Most of the simulations of this paper were performed on the University of Exeter's high performance computer ISCA.

-
- [1] A. Philbert, S. L. Lyantagaye, and G. Nkwengulila, *Adv. Entomol.* **02**, 120 (2014).
- [2] J. O'Neill *et al.*, available at https://amr-review.org/sites/default/files/160518_Final%20paper_with%20cover.pdf.
- [3] B. Mansoori, A. Mohammadi, S. Davudian, S. Shirjang, and B. Baradaran, *Adv. Pharm. Bull.* **7**, 339 (2017).
- [4] T. B. Kepler and A. S. Perelson, *Proc. Natl. Acad. Sci. USA* **95**, 11514 (1998).
- [5] S. Moreno-Gamez, A. L. Hill, D. I. Rosenbloom, D. A. Petrov, M. A. Nowak, and P. S. Pennings, *Proc. Natl. Acad. Sci. USA* **112**, E2874 (2015).
- [6] R. Hermsen, J. B. Deris, and T. Hwa, *Proc. Natl. Acad. Sci. USA* **109**, 10775 (2012).
- [7] P. Greulich, B. Waclaw, and R. J. Allen, *Phys. Rev. Lett.* **109**, 088101 (2012).
- [8] L. Rimbaud, J. Papaix, L. G. Barrett, J. J. Burdon, and P. H. Thrall, *Evol. Appl.* **11**, 1791 (2018).
- [9] R. Jullien and R. Botet, *Phys. Rev. Lett.* **54**, 2055 (1985).
- [10] M. Eden, in *Proceedings of the Fourth Berkeley Symposium on Mathematical Statistics and Probability*, edited by J. Neyman (Univ of California Press, Berkeley, 1961), Vol. 4, p. 223.
- [11] K. S. Korolev, M. Avlund, O. Hallatschek, and D. R. Nelson, *Rev. Mod. Phys.* **82**, 1691 (2010).
- [12] J.-T. Kuhr, M. Leisner, and E. Frey, *New J. Phys.* **13**, 113013 (2011).
- [13] W. Möbius, A. W. Murray, and D. R. Nelson, *PLoS Comput. Biol.* **11**, e1004615 (2015).
- [14] D. A. Beller, K. M. Alards, F. Tesser, R. A. Mosna, F. Toschi, and W. Möbius, *Europhys. Lett.* **123**, 58005 (2018).
- [15] M. Gralka and O. Hallatschek, *Elife* **8**, e44359 (2019).
- [16] See Supplemental Material at <http://link.aps.org/supplemental/10.1103/PhysRevE.108.044401> for (i) an in-depth discussion of the modified Eden model; (ii) a description of the specifics of simulations with this modified Eden model; (iii) analytical derivation of flat-front cluster height and width distributions; (iv) analytical derivation of escape region height; (v) analytical derivation of the random patch distribution percolation threshold; (vi) analytical derivation of the lattice patch distribution percolation threshold; (vii) videos and captions for videos. It also contains Refs. [9–15,18–24,29–31].
- [17] G. Ódor, *Rev. Mod. Phys.* **76**, 663 (2004).
- [18] W. Möbius, F. Tesser, K. M. Alards, R. Benzi, D. R. Nelson, and F. Toschi, *J. R. Soc. Interface.* **18**, 20210579 (2021).
- [19] W. Xia and M. F. Thorpe, *Phys. Rev. A* **38**, 2650 (1988).
- [20] E. Domany and W. Kinzel, *Phys. Rev. Lett.* **53**, 311 (1984).
- [21] J. Essam, *J. Phys. A: Math. Gen.* **22**, 4927 (1989).
- [22] OEIS Foundation Inc., The On-Line Encyclopedia of Integer Sequences, published electronically at <https://oeis.org/A080934> (2023).
- [23] OEIS Foundation Inc., The On-Line Encyclopedia of Integer Sequences, published electronically at <https://oeis.org/A080936> (2023).
- [24] S. Torquato, *Random Heterogeneous Materials: Microstructure and Macroscopic Properties* (Springer, New York, 2002) Chap. 4, p. 103.
- [25] H.-C. Chang and L.-C. Wang, [arXiv:1009.4322](https://arxiv.org/abs/1009.4322) [math.MG].
- [26] J. Paulose, J. Hermisson, and O. Hallatschek, *PLoS Genet.* **15**, e1007936 (2019).
- [27] J. Paulose and O. Hallatschek, *Proc. Natl. Acad. Sci. USA* **117**, 7584 (2020).
- [28] <https://github.com/tt386/assisted-percolation>.
- [29] M. Kardar, G. Parisi, and Y.-C. Zhang, *Phys. Rev. Lett.* **56**, 889 (1986).
- [30] E. W. Weisstein, Dyck path, (2020), published online at <https://mathworld.wolfram.com/DyckPath.html>.
- [31] W. R. Inc., Mathematica, Version 12.2, Champaign, IL, 2020.